Elsevier Editorial System(tm) for Journal of Biomechanics
Manuscript Draft

Manuscript Number: BM-D-13-00256R1

Title: Propagation of soft tissue artifacts to the center of rotation: a model for the correction of functional calibration techniques

Article Type: Full Length Article (max 3500 words)

Keywords: Soft tissue artifacts, functional calibration, center of rotation, gleno-humeral joint

Corresponding Author: Dr. Helios De Rosario,

Corresponding Author's Institution: Instituto de Biomecánica de Valencia

First Author: Helios De Rosario

Order of Authors: Helios De Rosario; Álvaro Page; Antonio Besa; Ángel Valera

Abstract: This paper presents a mathematical model for the propagation of errors in body segment kinematics to the location of the center of rotation. Three functional calibration techniques, usually employed for the gleno-humeral joint, are studied: the methods based on the pivot of the instantaneous helical axis (PIHA) or the finite helical axis (PFHA), and the "symmetrical center of rotation estimation" (SCoRE). A procedure for correcting the effect of soft tissue artifacts is also proposed, based on the equations of those techniques and a model of the artifact, like the one that can be obtained by double calibration. An experiment with a mechanical analogue was performed to validate the procedure and compare the performance of each technique. The raw error (between 57 and 68 mm) was reduced by a proportion of between 1:6 and less than 1:15, depending on the artifact model and the mathematical method. The best corrections were obtained by the SCoRE method. Some recommendations about the experimental setup for functional calibration techniques and the choice of a mathematical method are derived from theoretical considerations about the formulas and the results of the experiment.

Propagation of soft tissue artifacts to the center of rotation: a model for the correction of functional calibration techniques

Helios De Rosario [a,c,*], Álvaro Page [b,c], Antonio Besa[d], Ángel Valera[e]

[a] *Instituto de Biomecánica de Valencia, Valencia, Spain*

[b] *Departamento de Física Aplicada, Universitat Politècnica de València, Valencia, Spain*

[c] *CIBER de Bioingeniería, Biomateriales y Nanomedicina (CIBER-BBN), Spain*

[d] *Departamento de Ingeniería Mecánica y de Materiales, Universitat Politècnica de València, Valencia, Spain*

[e] *Instituto de Automática e Informática Industrial, Universitat Politècnica de València, Valencia, Spain*

* Corresponding author: Instituto de Biomecánica de Valencia, Universitat Politècnica de Valencia, Edificio 9C, Camino de Vera s/n, E-46022, Valencia, Spain. Tel: +34 963879160. Fax: +34 963879169. E-mail: helios.derosario@ibv.upv.es

Keywords: Soft tissue artifacts, functional calibration, center of rotation, gleno-humeral joint

Word count (Introduction through Discussion): 3,406

Number of tables: 3

Number of figures: 4

Abstract

This paper presents a mathematical model for the propagation of errors in body segment kinematics to the location of the center of rotation. Three functional calibration techniques, usually employed for the gleno-humeral joint, are studied: the methods based on the pivot of the instantaneous helical axis (PIHA) or the finite helical axis (PFHA), and the "symmetrical center of rotation estimation" (SCoRE). A procedure for correcting the effect of soft tissue artifacts is also proposed, based on the equations of those techniques and a model of the artifact, like the one that can be obtained by double calibration. An experiment with a mechanical analogue was performed to validate the procedure and compare the performance of each technique. The raw error (between 57 and 68 mm) was reduced by a proportion of between 1:6 and less than 1:15, depending on the artifact model and the mathematical method. The best corrections were obtained by the SCoRE method. Some recommendations about the experimental setup for functional calibration techniques and the choice of a mathematical method are derived from theoretical considerations about the formulas and the results of the experiment.

Notation

$\mathbf{a}^T$	Transpose of vector **a** (row vector)
$\mathbf{d}_{Xt}$	Displacement of point *X*
$\mathbf{e}_t$	Direction of the finite helical axis (unit vector)
$\mathbf{g}_t$	Position vector of the marker cluster center
$\mathbf{I}$	Identity matrix
$\mathbf{n}_t$	Direction of angular velocity/instantaneous helical axis (unit vector)
$\mathbf{P}\{.\}, \mathbf{S}\{.\}, \mathbf{T}\{.\}$	Matrix operators — see definitions in (2), (3), (9)
$\boldsymbol{q}_t = q_{wt} + \mathbf{q}_{vt}$	Quaternion (scalar and complex vector components)
$\mathbf{R}_t$	Rotation matrix
$\mathbf{r}_C$	Position vector of the center of rotation
t	Instant of time
$\mathbf{w}_t$	Angular velocity
$\mathbf{u}_{Xt}$	Direction of the velocity at point *X* (unit vector)
$\mathbf{v}_{Xt}$	Velocity at point *X*
$\delta\mathbf{a}$	Error (artifact) of the variable **a**
θ_t	Rotation angle
$\boldsymbol{\theta}_t$	Orientation vector $\left(=\theta_t\mathbf{e}_t\right)$
ξ	Phase variable
$\boldsymbol{\Omega}_t$	Rodrigues vector $\left(=\tan(\theta_t/2)\mathbf{e}_t\right)$

1

1. Introduction

The correct location of joints is crucial in many kinematic and kinetic analyses of human motion. This problem may be solved by predictive methods, based on the position of visible anatomical landmarks and regression equations, or by functional calibration techniques (FCT) that infer the joint position by analyzing a set of planned gestures (Della Croce et al., 2005). FCT are often preferred when the kinematic model chosen for the joint is a good approximation to reality and the range of motion is wide enough to ensure high accuracy. These two conditions are met by some human joints, most notably the hip and gleno-humeral joints, which may be modeled as "ball-and-socket" articulations and have the greatest ranges of motion (Cereatti et al., 2010; Karduna et al., 1996).

There is, however, controversy about the optimal mathematical approach to FCT. For the gleno-humeral joint in particular (GHJ), the International Society of Biomechanics (ISB) recommended calculating the pivot point of the instantaneous helical axes (Wu et al., 2005). A variation based on finite helical axes, to avoid inaccuracies and other problems in the derivation of velocities, has also been suggested (Halvorsen et al., 1999; Monnet et al., 2007). But in their comprehensive review, Ehrig et al. (2006) recommended the SCoRE method for estimating centers of rotation (CoR), on the basis of their results with numerical simulations. After that, others have compared the accuracy and repeatability of these methods applied to the GHJ, with diverging results (Lempereur et al., 2010; Monnet et al., 2007; Nikooyan et al., 2011).

This apparent inconsistency suggests that no method is generally superior, so it is necessary to take into account the nature of potential errors that may affect the

calculation of CoR, and how they are propagated by each method, before choosing a specific procedure. Many evaluations of FCT have been done with simulations that added random noise to a theoretical motion (Camomilla et al., 2006; Ehrig et al., 2006, 2011), but such simulations do not provide an adequate representation of actual errors in FCTs (Sangeux et al., 2011). Such errors are chiefly due to soft tissue artifacts (STA), which are simulated in some cases as "continuous noise" signals, with sinusoidal or Gaussian motions added to marker positions (Begon and Lacouture, 2005; Begon et al., 2007), although STA do not generally follow those patterns (Cerveri et al., 2005). Other simulations use real motion patterns of individual markers that have been observed in previous studies (Halvorsen et al., 1999), or measured in a deformable mechanical analogue (MacWilliams, 2008). However, real STA patterns can be modeled with fewer variables and independently of specific marker configurations, taking into account that the kinematic calculations are only affected by the rigid motion component, which is usually a function of the motion cycle (De Rosario et al., 2012).

The possibility of modeling STA as a function of joint kinematics (Camomilla et al., 2013) provides the opportunity of attempting their correction. This idea is the basis of techniques like the double calibration, whereby the motion of markers in the bone frame is linearly interpolated between previously measured positions at the ends of the motion cycle (Cappello et al., 2005; Brochard et al., 2011). The objective of this paper is to apply that idea to FCT, disentangling the underlying mathematics and defining formulas to correct CoR errors from STA models. Those formulas, validated with real data from a mechanical analogue, are presented as the basis for informed decisions about what method may be more adequate in different situations, and strategies to reduce it.

2. Material and methods

2.1. Mathematical methods

Three different ways of calculating the CoR were considered. The supplementary material contains some mathematical proofs of the statements that are succinctly presented in this section.

To simplify the calculations, the proximal segment was considered to be fixed, so that all the kinematic variables represent the relative motion of the distal segment, as seen in the proximal reference frame. Quaternions were preferred to other ways of representing rotations like matrices, Euler angles or orientation vectors, because they allowed more compact mathematical models of CoR errors, although it would be possible to derive such models from any other representation. For any unit quaternion, its complex vector and real scalar components, $\mathbf{q}_{vt} = q_x\mathbf{i} + q_y\mathbf{j} + q_z\mathbf{k}$ and q_{wt} respectively, were defined by the rotation angle θ_t and the direction of the helical axis $\mathbf{e}_t$ as follows (Chou, 1992):

$$\mathbf{q}_{vt} = \sin\left(\frac{\theta_t}{2}\right)\mathbf{e}_t, \quad q_w = \cos\left(\frac{\theta_t}{2}\right) \qquad (1)$$

The formulas for calculating the CoR presented in the following subsections include two special matrices. The skew-symmetric matrix $\mathbf{S}\{\mathbf{a}\}$ and the symmetric matrix $\mathbf{P}\{\mathbf{a}\}$ (where $\mathbf{a}$ is any column vector), which respectively define the cross product of $\mathbf{a}$ with another column vector, and the orthogonal projection on the plane normal to $\mathbf{a}$, scaled by the squared norm of that vector:

$$\mathbf{S}\{\mathbf{a}\} = \begin{pmatrix} 0 & -a_z & a_y \\ a_z & 0 & -a_x \\ -a_y & a_x & 0 \end{pmatrix} \quad : \quad \mathbf{S}\{\mathbf{a}\}\mathbf{b} = \mathbf{a} \times \mathbf{b} \qquad (2)$$

68 $$\mathbf{P}\{\mathbf{a}\} = \begin{pmatrix} a_y^2 + a_z^2 & -a_x a_y & -a_x a_z \\ -a_x a_y & a_x^2 + a_z^2 & -a_y a_z \\ -a_x a_z & -a_y a_z & a_x^2 + a_y^2 \end{pmatrix} = |\mathbf{a}|^2 \mathbf{I} - \mathbf{a}\mathbf{a}^T \quad : \quad \mathbf{P}\{\mathbf{a}\}\mathbf{b} = -\mathbf{a} \times (\mathbf{a} \times \mathbf{b})$$

69 (3)

70 *2.1.1. Pivot of Instantaneous Helical Axis (PIHA)*

71 The method recommended by the ISB consists of calculating all the locations of the
72 instantaneous helical axis during the calibration movements, and finding the nearest
73 point to them (Woltring, 1990). This is equivalent to solving the following matrix
74 equation:

75 $$\left(\sum_t \mathbf{P}\{\mathbf{n}_t\} \right) \mathbf{r}_C = \sum_t \mathbf{S}\{\mathbf{n}_t\} \mathbf{u}_{Ot}, \qquad (4)$$

76 where $\mathbf{r}_C$ is the position of the CoR, $\mathbf{n}_t$ is the unit vector of the angular velocity $\mathbf{w}_t$,
77 and $\mathbf{u}_{Ot}$ is the velocity at the origin "normalized" by the amount of angular velocity, i.e:

78 $$\mathbf{n}_t = \frac{\mathbf{w}_t}{|\mathbf{w}_t|} \qquad (5)$$

79 $$\mathbf{u}_{Ot} = \frac{\mathbf{v}_{Ot}}{|\mathbf{w}_t|} \qquad (6)$$

80 Since errors are very sensitive for low angular velocities, the frames where $|\mathbf{w}_t|$ is lower
81 than 0.25 rad/s are usually discarded (Monnet et al., 2007; Stokdijk et al., 2000).

82 *2.1.2. Pivot of Finite Helical Axes (PFHA)*

83 The second method is a variant of the former, where the target point is the pivot of the
84 finite helical axis (FHA), calculated from the displacement of skin markers with respect
85 to a fixed, reference position (Woltring, 1985). It is often used to calibrate the hip joint

86 center, but has also been applied to the GHJ (Lempereur et al., 2010). A weighting
87 factor equal to $\sin^2(\theta_t/2)$ may be used for an optimal compensation of small rotation
88 errors (Ehrig et al., 2006). Using quaternions and the translation of the origin $\mathbf{d}_{Ot}$, the
89 PFHA equation with this weighting factor is similar to (4):

90 $$\left(\sum_t \mathbf{P}\{\mathbf{q}_{vt}\}\right)\mathbf{r}_C = \sum_t \left(q_{wt}\mathbf{S}\{\mathbf{q}_{vt}\} + \mathbf{P}\{\mathbf{q}_{vt}\}\right)\frac{\mathbf{d}_{Ot}}{2}, \qquad (7)$$

91 *2.1.3. SCoRE*

92 The SCoRE method does not look for a fixed point, but a pair of points, one of each
93 linked segment, that keep a minimal distance during the motion, such that the CoR is
94 defined as the midpoint between them. The original equation defined by Ehrig et al.
95 (2006) may be rewritten as a function of the vectors and matrices described above:

96 $$\left(\sum_t \begin{pmatrix} \mathbf{P}\{\mathbf{q}_{vt}\} & -q_{wt}\mathbf{S}\{\mathbf{q}_{vt}\} \\ q_{wt}\mathbf{S}\{\mathbf{q}_{vt}\} & \mathbf{T}\{\boldsymbol{q}_t\} \end{pmatrix}\right)\begin{pmatrix} \mathbf{r}_C \\ \Delta_C \end{pmatrix} = \sum_t \begin{pmatrix} q_{wt}\mathbf{S}\{\mathbf{q}_{vt}\} + \mathbf{P}\{\mathbf{q}_{vt}\} \\ q_{wt}\mathbf{S}\{\mathbf{q}_{vt}\} - \mathbf{T}\{\boldsymbol{q}_t\} \end{pmatrix}\frac{\mathbf{d}_{Ot}}{2} \qquad (8)$$

97 where Δ_C is the vector that defines the distance between the two points, and $\mathbf{T}\{\boldsymbol{q}_t\}$ is
98 defined for the quaternion $\boldsymbol{q}_t$ as:

99 $$\mathbf{T}\{\boldsymbol{q}_t\} = \mathbf{I} - \mathbf{P}\{\mathbf{q}_{vt}\} = q_{wt}^2\mathbf{I} + \mathbf{q}_{vt}\,\mathbf{q}_{vt}^T \qquad (9)$$

100 *2.1.4. Error estimation*

101 If the CoR position were known beforehand, and the origin of coordinates were located
102 at that point, $\mathbf{r}_C$, $\mathbf{u}_{Ot}$, and $\mathbf{d}_{Ot}$ would ideally be null. Thus, in the presence of errors,
103 assuming that they are small with respect to the main motion, equations (4), (7) and (8)
104 may be used to calculate linear approximations of the CoR error $\delta\mathbf{r}_C$, as functions of the
105 error in velocities and translations at the theoretical CoR:

$$\left(\sum_t \mathbf{P}\{\mathbf{n}_t\}\right)\delta\mathbf{r}_C \approx \sum_t \left(\mathbf{S}\{\mathbf{n}_t\}\delta\mathbf{u}_{Ct}\right), \qquad (10)$$

$$\left(\sum_t \mathbf{P}\{\mathbf{q}_{vt}\}\right)\delta\mathbf{r}_C = \sum_t \left(q_{wt}\mathbf{S}\{\mathbf{q}_{vt}\} + \mathbf{P}\{\mathbf{q}_{vt}\}\right)\frac{\delta\mathbf{d}_{Ct}}{2}, \qquad (11)$$

$$\left(\sum_t \begin{pmatrix} \mathbf{P}\{\mathbf{q}_{vt}\} & -q_{wt}\mathbf{S}\{\mathbf{q}_{vt}\} \\ q_{wt}\mathbf{S}\{\mathbf{q}_{vt}\} & \mathbf{T}\{\boldsymbol{q}_t\} \end{pmatrix}\right)\begin{pmatrix} \delta\mathbf{r}_C \\ \delta\Delta_C \end{pmatrix} = \sum_t \begin{pmatrix} q_{wt}\mathbf{S}\{\mathbf{q}_{vt}\} + \mathbf{P}\{\mathbf{q}_{vt}\} \\ q_{wt}\mathbf{S}\{\mathbf{q}_{vt}\} - \mathbf{T}\{\boldsymbol{q}_t\} \end{pmatrix}\frac{\delta\mathbf{d}_{Ct}}{2} \qquad (12)$$

Note that in these formulas all the variables, including the kinematic errors $\delta\mathbf{u}_{Ct}$, $\delta\mathbf{d}_{Ct}$, are defined in the reference frame of the fixed segment. However, STA are often represented in a frame attached to the moving segment $\left({}^M\delta\mathbf{u}_{Ct},\ {}^M\delta\mathbf{d}_{Ct}\right)$. In such cases, those variables must be rotated before applying the equations:

$$\delta\mathbf{u}_{Ct} = \mathbf{R}_t\ {}^M\delta\mathbf{u}_{Ct} \quad ; \quad \delta\mathbf{d}_{Ct} = \mathbf{R}_t\ {}^M\delta\boldsymbol{d}_{Ct}, \qquad (13)$$

where $\mathbf{R}_t$ is the rotation matrix equivalent to $\boldsymbol{q}_t$.

2.2. Experimental validation

Given a model of the error in the kinematic variables, equations from (10) to (12) may be used to derive a model of the CoR error ($\delta\mathbf{r}_C$) and attempt its correction. This hypothesis was put to the test in an experiment with a mechanical analogue to the gleno-humeral joint: a metallic rod with a spherical joint at one of its ends, covered by flexible foam that was loosely attached to the bar and stuck to the fixed base, simulating a soft mass of tissue around the rigid bone (Figure 1). A rigid plate with 20 reflective markers was attached to the free end of the bar to have a STA-free measure of its motion. A 3x4 marker grid (100×166 mm) was fixed to the foam surface about 150 mm away from the joint center. The motion of this mechanism was recorded by 4 cameras with Kinescan/IBV at 50 frames per second.

126 The finite and instantaneous motions of both marker clusters were analyzed by vector
127 fields (Page et al., 2009b). That method gave the rotations of each marker cluster (i=1
128 for the rigid bar, i=2 for the foam) in terms of the Rodrigues vectors
129 $\mathbf{\Omega}_{it} = \tan(\theta_{it}/2)\mathbf{e}_{it}$, which were transformed to quaternions:

130 $$\mathbf{q}_{ivt} = \frac{\mathbf{\Omega}_{it}}{\sqrt{1+|\mathbf{\Omega}_{it}|^2}}, \quad q_{iwt} = \frac{1}{\sqrt{1+|\mathbf{\Omega}_{it}|^2}} \qquad (14)$$

131 The displacements and velocities at the origin of coordinates were calculated from their
132 homologous at the marker cluster centers (located at $\mathbf{g}_{i0}$ in the reference position, $\mathbf{g}_{it}$ in
133 instant t):

134 $$\mathbf{d}_{iOt} = \mathbf{d}_{iGt} - \mathbf{R}_{it}\mathbf{g}_{i0} + \mathbf{g}_{i0} \qquad (15)$$

135 $$\mathbf{v}_{iOt} = \mathbf{v}_{iGt} + \mathbf{g}_{it} \times \mathbf{w}_{it} \qquad (16)$$

136 The true CoR of the rigid bar was calculated by a preliminary calibration with the three
137 methods, combining various movements (symmetric and asymmetric flexion, elevation,
138 and half circumduction), each with three maximum angles, from 20º to 60º. The three
139 resulting CoR were averaged, and its accuracy was assessed by the SCoRE residual
140 (Ehrig et al., 2011). In subsequent calculations, the origin of the reference system was
141 translated to this average, "optimal" CoR.

142 For the experimental measure of the CoR, three typical calibration motions were used,
143 as defined in Table 1 (Leardini et al., 1999; Piazza et al., 2004). The motions of the bar
144 and foam marker sets were recorded simultaneously. The foam markers were used to
145 calculate the experimental CoR with STA, using the three methods. Since the origin of
146 coordinates was located at the theoretical CoR, the resulting values were a measure of
147 the CoR error.

148 The finite components of the STA in the moving frame $\left({}^{M}\delta\boldsymbol{q}_t,\ {}^{M}\delta\mathbf{d}_{Ct}\right)$ were calculated
149 from the relative motion between both marker sets (De Rosario et al., 2012). The
150 corresponding field of velocities was estimated from their derivatives, considering small
151 STA rotations $\left({}^{M}\delta\boldsymbol{q}_t \approx 1+{}^{M}\delta\mathbf{q}_{vt}\right)$:

152 $$ {}^{M}\delta\mathbf{w}_t \approx 2\left({}^{M}\delta\dot{\mathbf{q}}_{vt}\right) \qquad (17)$$

153 $$ {}^{M}\delta\mathbf{v}_{Ct} \approx {}^{M}\delta\dot{\mathbf{d}}_{Ct} - {}^{M}\delta\mathbf{w}_t \times {}^{M}\delta\mathbf{d}_{Ct} \qquad (18)$$

154 The displacement of the markers in the reference frame of the bar was measured, and
155 the rotation artifact was compared to *in vivo* results published by Hamming et al.
156 (2012).

157 Assuming a systematic relation between the STA and the motion cycle, two artifact
158 models were defined as functions of a phase variable (ξ), determined for each gesture as
159 presented in Table 1. In planar motions (Flex., Elev.), ξ was the main coordinate of the
160 orientation vector $\boldsymbol{\theta}_t$. For Circ., which had an oscillating FHA, ξ was a function of the
161 main coordinates of $\boldsymbol{\theta}_t$, which kept a quasi-sinusoidal progression over the motion
162 cycle.

163 Using this phase variable, an optimal estimation of the STA was attempted by fitting
164 ${}^{M}\delta\boldsymbol{q}_t,\ {}^{M}\delta\mathbf{d}_{Ct}$ to functional averages with one functional degree of freedom, as done by
165 De Rosario et al. (2012). That model was used to confirm the validity of the equations,
166 although it required having detailed knowledge of the STA during the whole
167 measurement, which is not the normal situation. A simpler and more realistic
168 estimation, analogous to what may be obtained by double calibration, was calculated by
169 fitting piecewise linear regression equations:

$$\mathbf{f}_t = \beta_0 + \beta_1 \xi, \qquad (19)$$

for $\mathbf{f}_t = {}^M\delta\boldsymbol{q}_t, {}^M\delta\mathbf{d}_{Ct}$, where β_0, β_1 were fitted separately for each motion, and for positive and negative values of ξ. Only 5% of the instants around the reference and end postures (smallest and greatest absolute values of ξ, respectively) were used for fitting the linear model, to simulate the double calibration procedure. The normalized infinitesimal parameters $\left({}^M\delta\mathbf{n}_t, {}^M\delta\mathbf{u}_{Ct}\right)$ were derived from their finite counterparts for both the functional average and the linear interpolation (Page et al., 2009a, 2010), and all the variables were rotated to express them in the fixed reference frame.

The goodness-of-fit was measured in both cases for the translational components $\left(\delta\mathbf{d}_{Ct}, \delta\mathbf{u}_{Ct}\right)$, which are the ones that influenced the CoR error, using the coefficient of determination R^2, i.e. the ratio between the variance explained by the STA model and the total variance of the STA parameters.

Then, both STA models were used to predict the CoR errors from equations (10) to (12), and they were subtracted from the raw results to obtain "corrected" centers. For each set of results (uncorrected CoR, values corrected by the functional average model, and values corrected by the linear model), a Chi-square test was used to assess whether the differences between the three methods (PIHA, PFHA, and SCoRE) were significant. The test statistic was

$$T = 2\frac{Var\left(\left|\mathbf{r}_{Cm}\right|\right)}{\varepsilon^2}, \qquad (20)$$

where $\mathbf{r}_{Cm}$ represented the result of each method, and ε was the expected size of accidental CoR errors, estimated as half the SCoRE residual of the reference CoR.

3. Results

The SCoRE residual of the "true" CoR calculated in the preliminary calibration was 6.6 mm, i.e. $\varepsilon = 3.3$ mm. The values obtained by PIHA, PFHA and SCoRE were at 4.1 mm, 3.2 mm, and 1.2 mm from the average reference point, respectively (the SCoRE center was located in between the other two).

Figure 2 shows the distribution of marker displacements in the moving frame. The interquartile ranges were between 10 and 20 mm, and the maximum values were below 30 mm for the top and medial rows, but there were peaks between 30 and 50 mm for the bottom row. Table 2 compares the measured rotation artifacts with the humerus rotation errors reported by Hamming et al. (2012).

Figures 3 and 4 show the observed and fitted values of the STA parameters that affected the CoR error: the relative translation and the normalized velocity at the theoretical CoR, in the moving reference frame. The fitted curves explained most of the observed variance in $\delta\mathbf{d}_{Ct}$ ($R^2 = 0.971$ for the functional average, 0.895 for the linear interpolation). The fit of $\delta\mathbf{u}_{Ct}$ was poorer ($R^2 = 0.633$ for the functional average, 0.619 for the linear interpolation).

Table 3 shows the experimental CoR errors for each method, before correcting the STA effects and after correcting them by functional average and linear interpolation. It may be seen that the uncorrected CoR had a large error (between 57.2 and 68.3 mm) in the *Z*-coordinate (the medio-lateral axis in the shoulder analogue), which was drastically reduced to less than 11 mm with both corrections.

The highest and lowest errors varied across methods for each set of calculations, although PIHA gave the highest in two cases (uncorrected and linear interpolation), and

SCoRE the lowest in both corrections. To evaluate these differences in statistical terms, Table 3 also presents the *T*-statistics defined in (20). Their comparison with a χ^2_2 distribution shows that the resulting error was not significantly different between the three methods $(p > 0.05)$, specially after the corrections.

4. Discussion

The effect of marker errors in the calculation of rotation centers has already been studied analytically for planar motion (Bryant et al., 1984; Crisco III et al., 1994), and also for 3-D instantaneous kinematics (Page et al., 2007). This study has extended that approach to the analysis of the 3-D CoR, giving explicit error formulas for three FCT methods that are usually applied to the GHJ (PIHA, PFHA, and SCoRE), and proposing a procedure to correct STA effects that can be summarized in three steps:

1. Measure the motion and obtain a first estimation of the CoR by the normal procedure, with equations (4), (7), or (8) — or equivalent formulas with the preferred rotation formalism.

2. Define a model the translational component of the STA at the estimated CoR $(\delta\mathbf{d}_{Ct}, \delta\mathbf{u}_{Ct})$.

3. Repeat step #1, replacing $\mathbf{u}_{Ot}$ or $\mathbf{d}_{Ot}$ by $\delta\mathbf{u}_{Ct}$ or $\delta\mathbf{d}_{Ct}$ in the corresponding formula, and subtract the result from the first estimation of the CoR.

The properties of the error model and the correction method were illustrated by an experiment with a mechanical analogue, a frequent resource for experimental validations of mathematical procedures (Camomilla et al., 2006; MacWilliams, 2008;

Piazza et al., 2001), since they facilitate testing multiple configurations and movements, with rigorous control of the errors.

An important point is that the only element of STA that matters in FCT is the translational component of the artifact (displacement or velocity, depending on the algorithm) at the CoR. However, rotation or angular velocity errors also create translational errors proportional to the distance between the CoR and the marker cluster center (Crisco III et al., 1994; Woltring et al., 1985, 1990). Thus, the recommendation of placing the markers away from the joint to increase the signal-to-noise ratio (Kratzenstein et al., 2012) should be approached cautiously, to avoid large marker eccentricities. Related to this, it is notable that the cluster of foam markers was mainly separated from the CoR in the direction of the *Z*-axis, and the CoR error in that axis (before correcting it) was about 10 times the error in the other directions.

Regarding the different calculation techniques, the most important formal distinction is between the velocity-based method (PIHA) and those based on positions (PFHA, SCoRE). The latter may be preferred for noisy data, where velocities cannot be derived accurately. Likewise, velocity errors may also increase in calibrations that include quick, "explosive" gestures (Begon et al., 2007). On the other hand, if the STA is a displacement of the markers that remains approximately constant during the central part of the motion cycle, and its main increment occurs at the ends of the cycle, PIHA may be less sensitive to such errors than position-based methods. In the reported experiment, uncorrected errors were higher for PIHA, and the estimations of velocity errors were worse fitted to the actual STA than the finite translation error. As could be expected from that, the correction of the CoR by the PIHA method was outperformed by at least one of the other methods, although the differences were not significant.

The difference between PFHA and SCoRE is more subtle: both are optimizations of similar objective functions (a point of minimum relative displacement, and a couple of points with minimum separation during the measurement, respectively). SCoRE is advantageous when the error comes from both linked segments, since it does not introduce a bias depending on what segment is considered "fixed" in the analysis. In the reported experiment, one of the segments was actually fixed, so that advantage could not be noticed. Accordingly, although SCoRE performed better than PFHA for both error corrections, the differences between PFHA and SCoRE were not significant, as also happened in previous studies with simulated and real data (Ehrig et al., 2006; Lempereur et al., 2010). In fact, the comparison of equations (7) and (8) shows that PFHA and SCoRE are mathematically equivalent if the motion is perfectly symmetrical with respect to the reference position ($\Sigma_t \mathbf{S}\{\mathbf{q}_{vt}\}$ would add up to zero in that case).

Finally, it has been shown how the correction from estimated STA patterns may drastically reduce the error of the CoR. In the example experiment, the proportion between corrected and uncorrected errors ranged from 1:6 to 1:15. Those ratios were better than the ones obtained by improving the marker cluster design (Kratzenstein et al., 2012), solidification procedures (Begon and Lacouture, 2005), or different variants of the Optimal Common Shape Technique (Heller et al., 2011).

Nevertheless, such quantitative results must be treated with caution, since they come from an artificial experimental setup, which may not represent the actual kinematic characteristics of human motion and artifacts in real conditions. In this case, the relative motion of the markers was similar to typical values of human STA in the top and central rows, and within reported ranges but larger than usual in the bottom row (Leardini et al., 2005; Stagni et al., 2005). The average STA rotations were also normal, although the

peak values of the elevation angle and plane were higher than *in vivo* results. Likewise, the uncorrected CoR error (over 57 mm) was greater than the errors reported for human joints using the same methods, which are normally lower than 40 mm (Cereatti et al., 2009). The relative performance of the error correction method might be overestimated due to such great initial errors, but in any case, the error of the corrected CoR (between 3.6 and 11 mm) was lower than the 15-to-20 mm error reported for *in vivo* measures of the GHJ (Lempereur et al., 2010; Nikooyan et al., 2011), in spite of the large initial error.

An additional advantage of this method for estimating and correcting CoR errors is that it can be implemented with the same computer programs that are used for calculating its position by standard procedures. The only challenging part is obtaining a model of the STA. But it has been shown that even simple estimations like a piecewise linear interpolation achieved excellent results. Thus, this method can be applied to obtain improved estimations of the CoR of real joints by means of the normal FCT procedures, plus a double calibration or other linear approximations of STA (Camomilla et al., 2013).

Acknowledgements

This work has been funded by the Spanish Government (Grants DPI2009-13830-C02-01, DPI2009-13830-C02-02, DPI2010-20814-C02-01, DPI2010-20814-C02-02).

References

Begon, M., Lacouture, P., 2005. Solidification procedure adapted to locating joint centre. Computer Methods in Biomechanics and Biomedical Engineering 8, 23–24.

Begon, M., Monnet, T., Lacouture, P., 2007. Effects of movement for estimating the hip joint centre. Gait & Posture 25, 353–359.

Brochard, S., Lempereur, M., Rémy-Néris, O., 2011. Double calibration: An accurate, reliable and easy-to-use method for 3D scapular motion analysis. Journal of Biomechanics 44, 751–754.

Bryant, J.T., Wevers, H.W., Lowe, P.J., 1984. One parameter model for error in instantaneous centre of rotation measurements. Journal of Biomechanics 17, 317–323.

Camomilla, V., Cereatti, A., Chèze, L., Cappozzo, A., 2013. A hip joint kinematics driven model for the generation of realistic thigh soft tissue artefacts. Journal of Biomechanics 46, 625–630.

Camomilla, V., Cereatti, A., Vannozzi, G., Cappozzo, A., 2006. An optimized protocol for hip joint centre determination using the functional method. Journal of Biomechanics 39, 1096–1106.

Cappello, A., Stagni, R., Fantozzi, S., Leardini, A., 2005. Soft tissue artifact compensation in knee kinematics by double anatomical landmark calibration: performance of a novel method during selected motor tasks. Biomedical Engineering, IEEE Transactions on 52, 992–998.

Cereatti, A., Donati, M., Camomilla, V., Margheritini, F., Cappozzo, A., 2009. Hip joint centre location: An ex vivo study. Journal of Biomechanics 42, 818–823.

Cereatti, A., Margheritini, F., Donati, M., Cappozzo, A., 2010. Is the human acetabulofemoral joint spherical? Journal of Bone and Joint Surgery - British Volum 92-B, 311–314.

Cerveri, P., Pedotti, A., Ferrigno, G., 2005. Kinematical models to reduce the effect of skin artifacts on marker-based human motion estimation. Journal of Biomechanics 38, 2228–2236.

Chou, J.C.K., 1992. Quaternion kinematic and dynamic differential equations. IEEE Transactions on Robotics and Automation 8, 53–64.

Crisco III, J.J., Chen, X., Panjabi, M.M., Wolfe, S.W., 1994. Optimal marker placement for calculating the instantaneous center of rotation. Journal of Biomechanics 27, 1183–1187.

De Rosario, H., Page, Á., Besa, A., Mata, V., Conejero, E., 2012. Kinematic description of soft tissue artifacts: quantifying rigid versus deformation components and their relation with bone motion. Medical & Biological Engineering & Computing 50, 1173–1181.

Della Croce, U., Leardini, A., Chiari, L., Cappozzo, A., 2005. Human movement analysis using stereophotogrammetry: Part 4: assessment of anatomical landmark misplacement and its effects on joint kinematics. Gait & posture 21, 226–237.

Ehrig, R.M., Heller, M.O., Kratzenstein, S., Duda, G.N., Trepczynski, A., Taylor, W.R., 2011. The SCoRE residual: A quality index to assess the accuracy of joint estimations. Journal of Biomechanics 44, 1400–1404.

Ehrig, R.M., Taylor, W.R., Duda, G.N., Heller, M.O., 2006. A survey of formal methods for determining the centre of rotation of ball joints. Journal of Biomechanics 39, 2798–2809.

Halvorsen, K., Lesser, M., Lundberg, A., 1999. A new method for estimating the axis of rotation and the center of rotation. Journal of Biomechanics 32, 1221–1227.

Hamming, D., Braman, J.P., Phadke, V., LaPrade, R.F., Ludewig, P.M., 2012. The accuracy of measuring glenohumeral motion with a surface humeral cuff. Journal of Biomechanics 45, 1161–1168.

Heller, M.O., Kratzenstein, S., Ehrig, R.M., Wassilew, G., Duda, G.N., Taylor, W.R., 2011. The weighted optimal common shape technique improves identification of the hip joint center of rotation in vivo. Journal of Orthopaedic Research 29, 1470–1475.

Karduna, A.R., Williams, G.R., Iannotti, J.P., Williams, J.L., 1996. Kinematics of the glenohumeral joint: Influences of muscle forces, ligamentous constraints, and articular geometry. Journal of Orthopaedic Research 14, 986–993.

Kratzenstein, S., Kornaropoulos, E.I., Ehrig, R.M., Heller, M.O., Pöpplau, B.M., Taylor, W.R., 2012. Effective marker placement for functional identification of the centre of rotation at the hip. Gait & Posture 36, 482–486.

Leardini, A., Cappozzo, A., Catani, F., Toksvig-Larsen, S., Petitto, A., Sforza, V., Cassanelli, G., Giannini, S., 1999. Validation of a functional method for the estimation of hip joint centre location. Journal of Biomechanics 32, 99–103.

Leardini, A., Chiari, L., Croce, U.D., Cappozzo, A., 2005. Human movement analysis using stereophotogrammetry: Part 3. Soft tissue artifact assessment and compensation. Gait & Posture 21, 212–225.

Lempereur, M., Leboeuf, F., Brochard, S., Rousset, J., Burdin, V., Rémy-Néris, O., 2010. In vivo estimation of the glenohumeral joint centre by functional methods: Accuracy and repeatability assessment. Journal of Biomechanics 43, 370–374.

MacWilliams, B.A., 2008. A comparison of four functional methods to determine centers and axes of rotations. Gait & Posture 28, 673–679.

Monnet, T., Desailly, E., Begon, M., Vallée, C., Lacouture, P., 2007. Comparison of the SCoRE and HA methods for locating in vivo the glenohumeral joint centre. Journal of Biomechanics 40, 3487–3492.

Nikooyan, A.A., Van der Helm, F.C.T., Westerhoff, P., Graichen, F., Bergmann, G., (Dirkjan) Veeger, H.E.J., 2011. Comparison of two methods for in vivo estimation of the glenohumeral joint rotation center (GH-JRC) of the patients with shoulder hemiarthroplasty. PLoS ONE 6, e18488.

Page, Á., Gálvez, J.A., De Rosario, H., Mata, V., Prat, J., 2010. Optimal average path of the instantaneous helical axis in planar motions with one functional degree of freedom. Journal of Biomechanics 43, 375–378.

Page, Á., Gálvez, J.A., De Rosario, H., Mata, V., Baydal, J.M., 2009a. Optimal average path of the instantaneous screw axis in 3D human movements. In: ESMC2009, 7th EUROMECH Solid Mechanics Conference.

Page, Á., Mata, V., Hoyos, J.V., Porcar, R., 2007. Experimental determination of instantaneous screw axis in human motions. Error analysis. Mechanism and Machine Theory 42, 429–441.

Page, Á., De Rosario, H., Mata, V., Atienza, C., 2009b. Experimental Analysis of Rigid Body Motion. A Vector Method to Determine Finite and Infinitesimal Displacements From Point Coordinates. Journal of Mechanical Design 131, 031005.

Piazza, S.J., Okita, N., Cavanagh, P.R., 2001. Accuracy of the functional method of hip joint center location: effects of limited motion and varied implementation. Journal of Biomechanics 34, 967–973.

Piazza, S.J., Erdemir, A., Okita, N., Cavanagh, P.R., 2004. Assessment of the functional method of hip joint center location subject to reduced range of hip motion. Journal of Biomechanics 37, 349–356.

Sangeux, M., Peters, A., Baker, R., 2011. Hip joint centre localization: Evaluation on normal subjects in the context of gait analysis. Gait & Posture 34, 324–328.

Stagni, R., Fantozzi, S., Cappello, A., Leardini, A., 2005. Quantification of soft tissue artefact in motion analysis by combining 3D fluoroscopy and stereophotogrammetry: a study on two subjects. Clinical Biomechanics 20, 320–329.

Stokdijk, M., Nagels, J., Rozing, P.M., 2000. The glenohumeral joint rotation centre in vivo. Journal of Biomechanics 33, 1629–1636.

Woltring, H.J., 1990. Data processing and error analysis. In: Cappozzo, A., Berme, P. (Eds.), Biomechanics of Human Movement: Applications in Rehabilitation, Sport and Ergonomics. Worthington: Bertec Corporation, pp. 203–227.

Woltring, H.J., Huiskes, R., Lange, A. de, Veldpaus, F.E., 1985. Finite centroid and helical axis estimation from noisy landmark measurements in the study of human joint kinematics. Journal of Biomechanics 18, 379–389.

Wu, G., van der Helm, F.C.T., (DirkJan) Veeger, H.E.J., Makhsous, M., Van Roy, P., Anglin, C., Nagels, J., Karduna, A.R., McQuade, K., Wang, X., Werner, F.W., Buchholz, B., 2005. ISB recommendation on definitions of joint coordinate systems of various joints for the reporting of human joint motion—Part II: shoulder, elbow, wrist and hand. Journal of Biomechanics 38, 981–992.

Table 1. Description of the three motions used for the FCT and the variable that represented the cycle progression.

Motion	Description	Phase variable (ξ)
Flex.	Five asymmetric flexion-extension cycles around the *Z*-axis, from -15º to 45º	*Z*-coordinate of $\boldsymbol{\theta}_t$ (θ_z)
Elev.	Five elevation cycles around the *X*-axis, from 0º to 40º	*X*-coordinate of $\boldsymbol{\theta}_t$ (θ_x)
Circ.	Five half circumduction cycles around the *Y*-axis, at 25º of elevation	Angle of θ_z wrt θ_x

Table 2. Errors in Euler angles (XZ'Y'' sequence) of the measured prototype, compared with *in vivo* measures of the humerus.

		Elevation angle (X)	Elevation plane (Z')	Axial rotation (Y'')
Mean	*In vivo*[1]	2.3	1.2	5.3
	Prototype	1.2	2.4	2.3
Peak	*In vivo*[1]	4.0	2.1	6.3
	Prototype	7.1	4.4	5.4

[1] For various flexion and abduction movements (Hamming et al., 2012)

Table 3. CoR errors: uncorrected, and corrected by subtraction of the estimated STA effects (functional average and linear interpolation estimates). The *T*-statistic and *p*-values refer to each group of errors.

	X (mm)	Y (mm)	Z (mm)	norm (mm)	*T*	*p*
Uncorrected						
PIHA	-5.0	-6.3	67.8	68.3	5.752	0.056
PFHA	-4.3	1.2	57.0	57.2		
SCoRE	-5.3	-4.6	62.4	62.8		
Functional average						
PIHA	-2.7	0.6	5.8	6.4	1.099	0.577
PFHA	-2.7	7.9	-0.5	8.4		
SCoRE	-2.6	0.9	2.3	3.6		
Linear interpolation						
PIHA	-5.1	-1.1	10.2	11.0	0.869	0.647
PFHA	-4.8	6.5	1.9	8.5		
SCoRE	-4.1	-1.2	4.6	6.7		

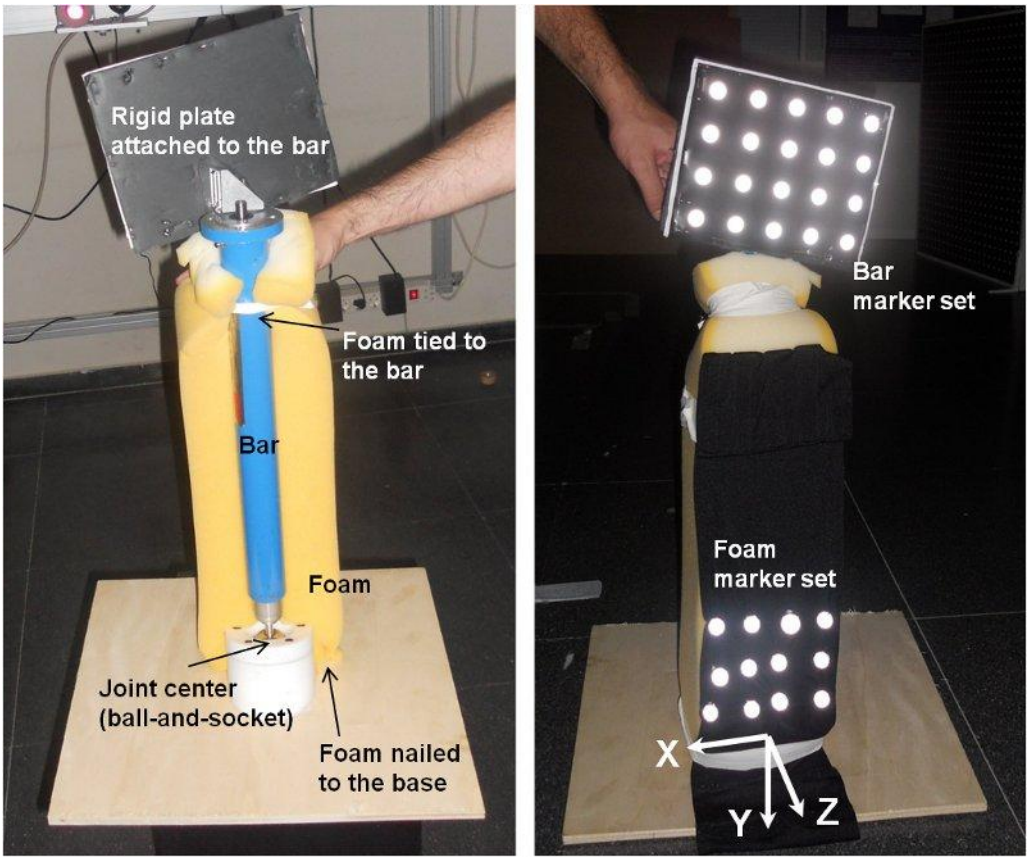

Figure 1. Experiment setup

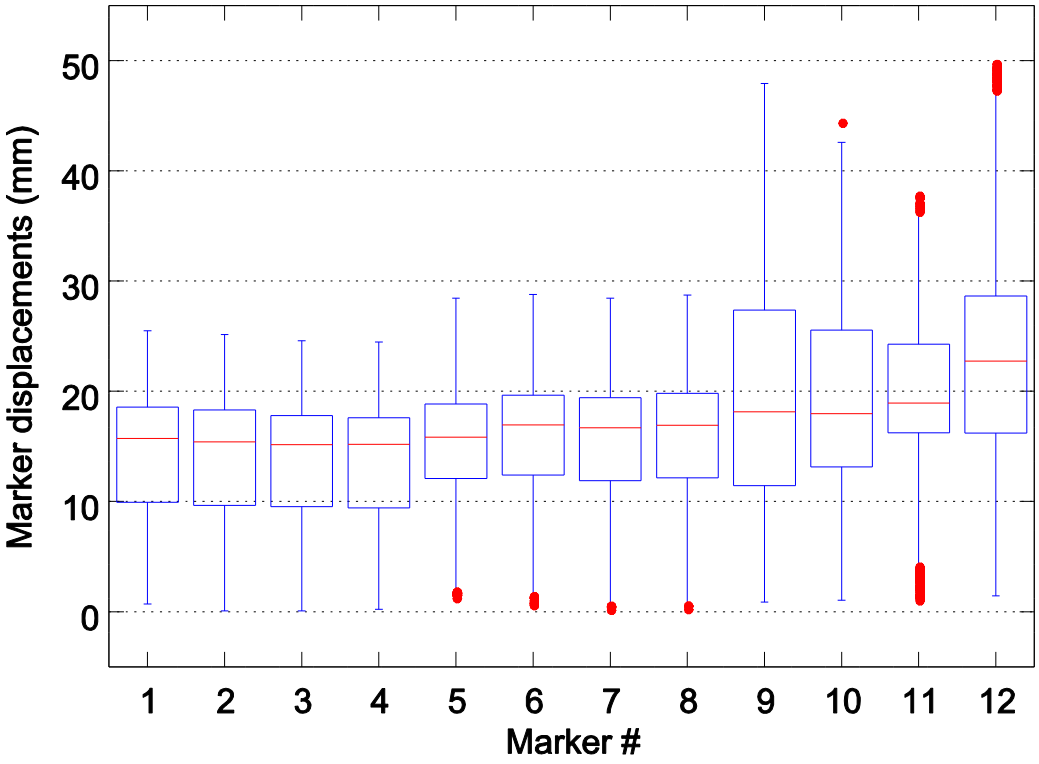

Figure 2. Displacements of the foam markers in the bar-embedded frame (sorted by rows of the marker grid).

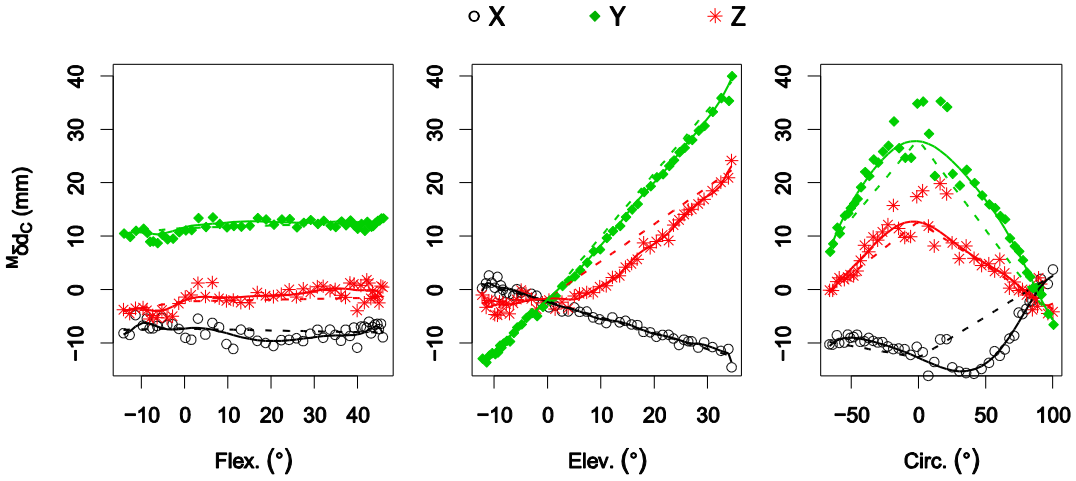

Figure 3. Observed and fitted translations associated with the STA at the CoR, seen in the reference frame of the moving segment. Solid lines: functional average; dashed lines: linear interpolation.

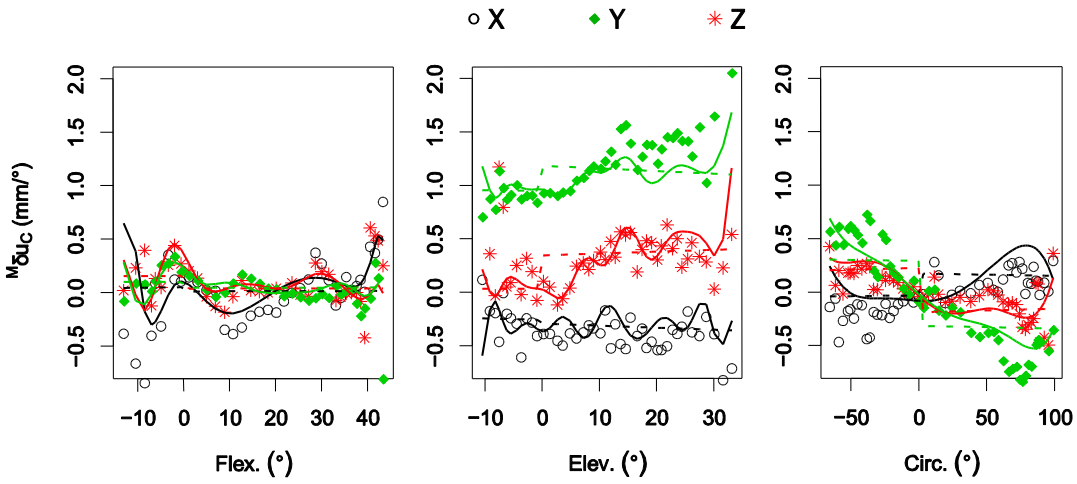

Figure 4. Observed and fitted normalized velocities of the STA at the CoR, seen in the reference frame of the moving segment. Solid lines: functional average; dashed lines: linear interpolation.

Figure 1

Click here to download high resolution image

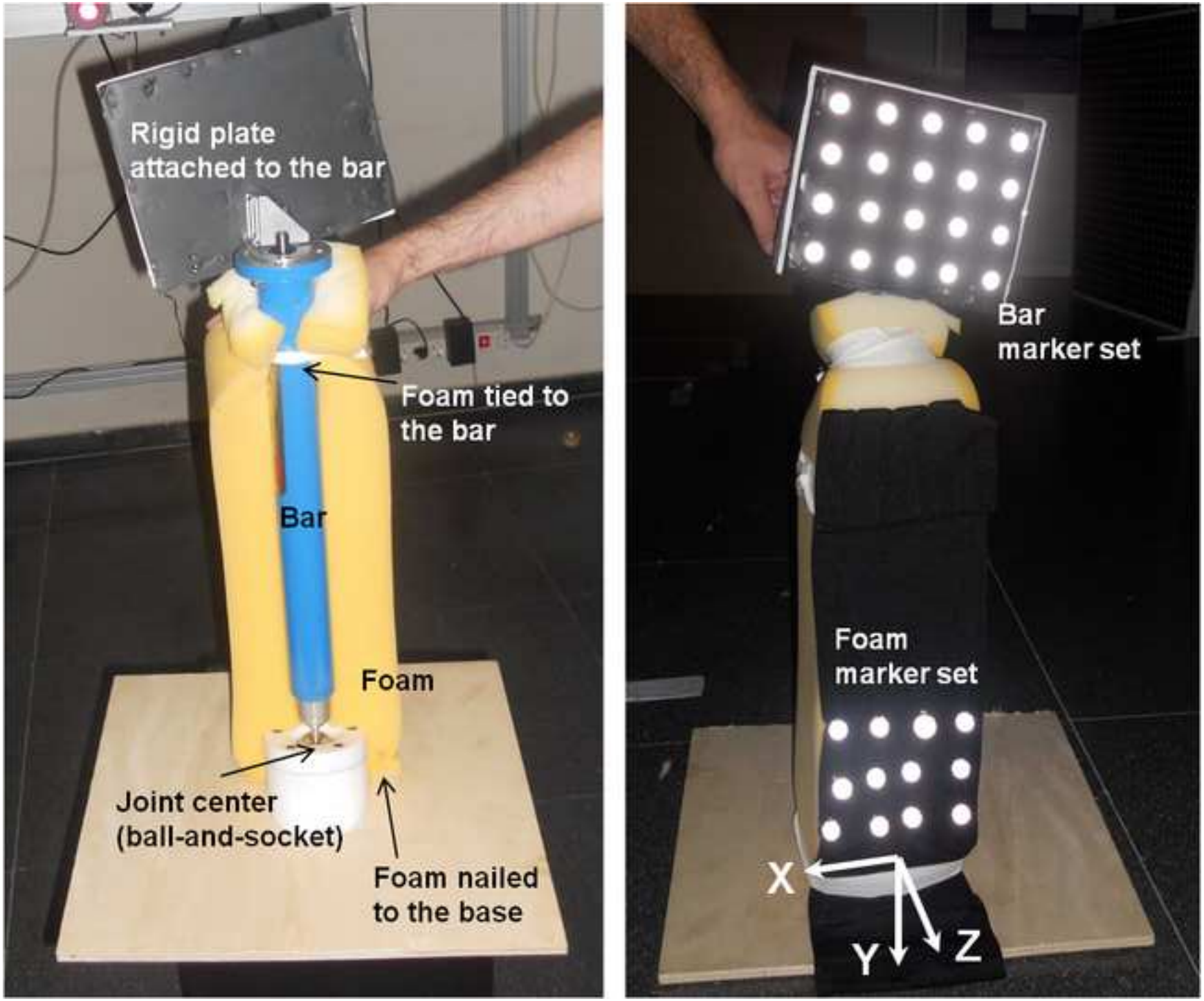

Figure 2

Click here to download Figure: figure2.eps

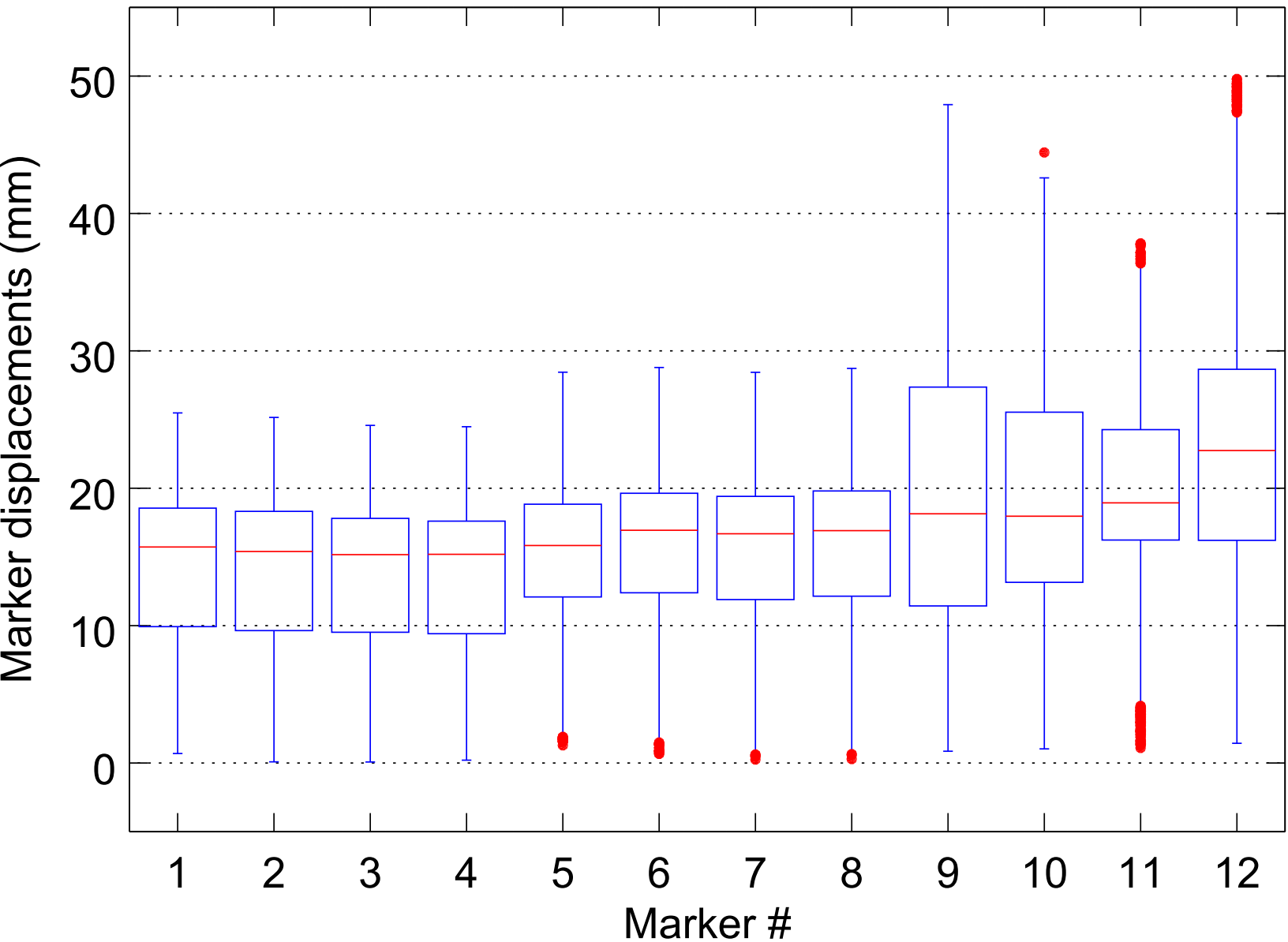

Figure 3

Click here to download Figure: figure3.eps

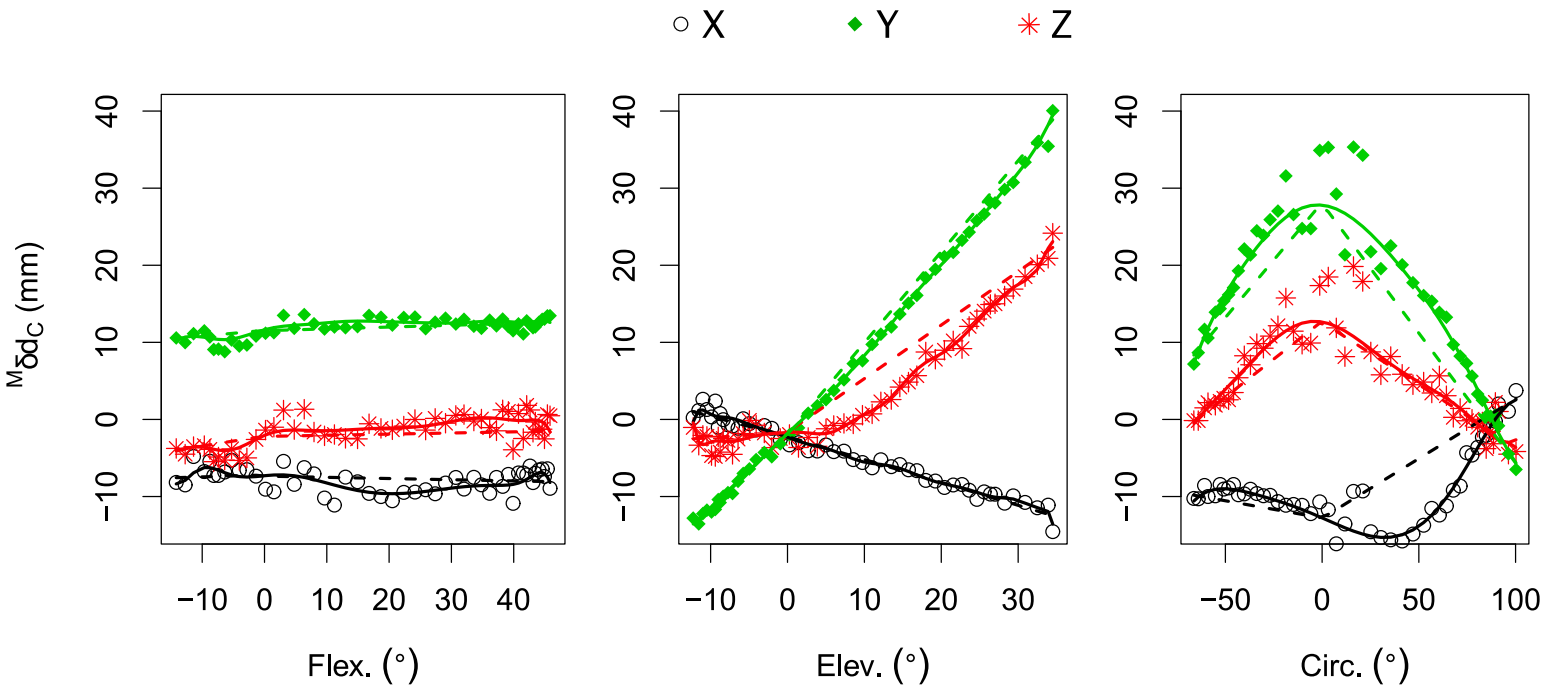

Figure 4

Click here to download Figure: figure4.eps

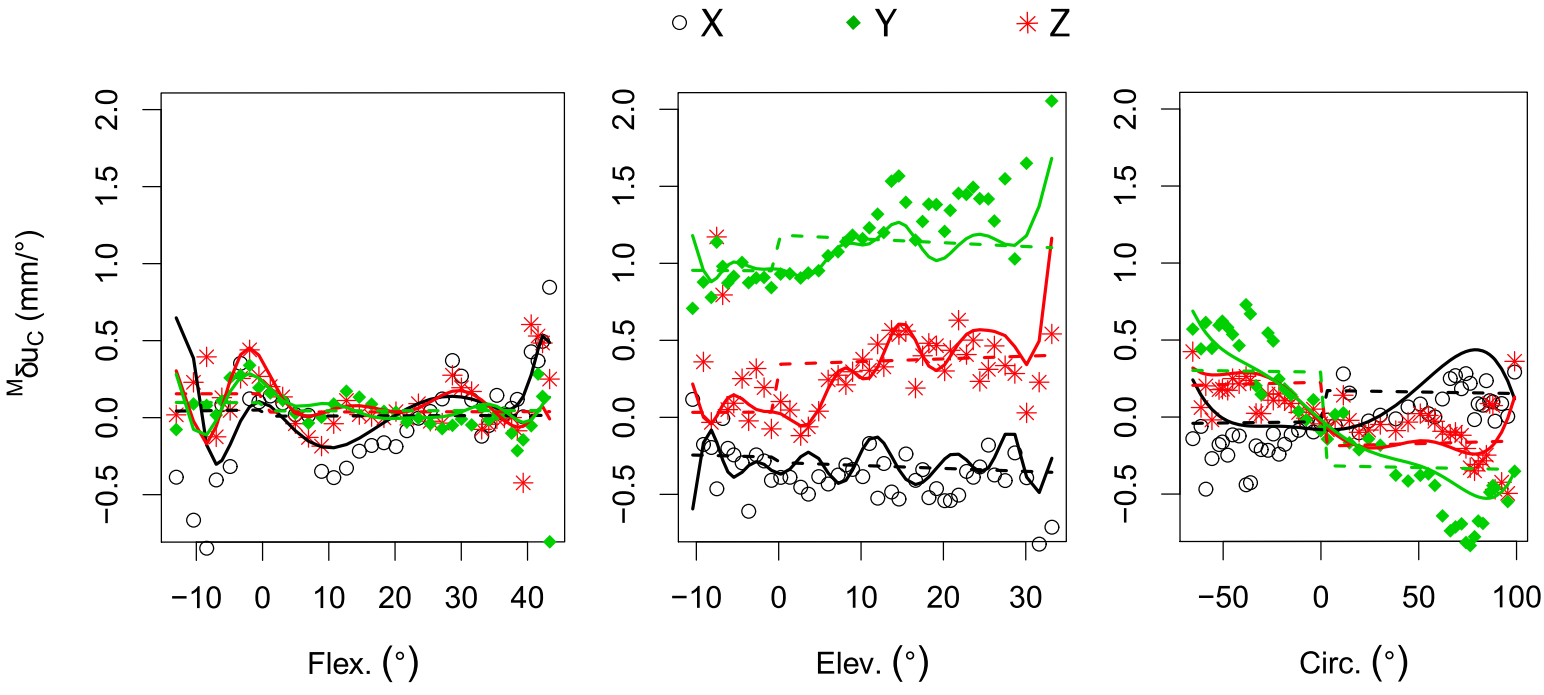

Supplementary Material

Click here to download Supplementary Material: STA_FCT.pdf

Conflict of interest statement

The authors of this paper have no conflict of interest.